Hindawi
International Journal of RF and Microwave Computer-Aided Engineering
Volume 2024, Article ID 9923732, 13 pages
https://doi.org/10.1155/2024/9923732

Research Article

A Novel Antenna Design of Compact HF and UHF Passive RFID Tags with Interconnected Structure for Energy Harvesting and Tracking Systems

Supakit Kawdungta,[1] **Theerayut Mhunkaew**,[1] **Danai Torrungrueng**,[2] **and Hsi-Tseng Chou**[3]

[1]*Faculty of Engineering, Rajamangala University of Technology Lanna, Chiang Mai, Thailand*
[2]*Research Center of Innovation Digital and Electromagnetic Technology, Department of Teacher Training in Electrical Engineering, Faculty of Technical Education, King Mongkut's University of Technology North Bangkok, Bangkok 10800, Thailand*
[3]*Graduate Institute of Communication Engineering, National Taiwan University, Taipei 10617, Taiwan*

Correspondence should be addressed to Danai Torrungrueng; dtg@ieee.org

Received 5 August 2023; Revised 26 November 2023; Accepted 5 January 2024; Published 24 January 2024

Academic Editor: Chow-Yen-Desmond Sim

We propose a new dual-band passive RFID tag antenna design by combining a rectangular spiral coil and patch-meander-line dipole with an interconnected structure. This design enables operation in high-frequency (HF) and ultra-high-frequency (UHF) RFID systems, suitable for energy harvesting and tracking applications. The simulations by the CST full-wave software demonstrate conjugate impedance matching between the tag antenna and two RFID tag chips. At 13.56 MHz (HF), the tag antenna exhibits an inductive reactance of 422.79 Ω, while at 922.5 MHz (UHF), it presents an impedance of $9.41 + j174.96\ \Omega$. The antenna generates a maximum magnetic field intensity of 0.5 A/m and omnidirectional electromagnetic fields with an antenna realized gain of -4.26 dBi at 922.5 MHz. We also analyze the impact of the tag antenna combination using numerical software. Furthermore, we fabricate a prototype tag antenna and validate its performance with RFID readers. The proposed tag antenna achieves the maximum read ranges of 11 cm and 6.9 m for the HF (13.56 MHz) and UHF (920-925 MHz) bands, respectively, accompanied by the energy harvesting of 1.48 volts at the HF band by the coupling magnetic field received by the HF antenna to the chip ST25DV04K at the output voltage pin.

1. Introduction

Radiofrequency identification (RFID) systems are popularly employed to wirelessly identify objects by extracting the information from the embedded identification tags. Passive RFID tags are particularly welcomed for the advantage of without implementing batteries in them, where the operations are performed by imposing radio waves to illuminate the tags and provide the required power for data access. Compared to wired systems, RFID systems do not require a wire connection and allow non-line-of-sight data access. Moreover, the data access from the tags is bidirectionally read/written possibly. They are reusable, durable, and highly secured. As a result, passive RFID tags are broadly used in many short-range applications to identify people and objects. Some famous applications include intelligent highway toll-collection systems [1] and their extension in parking-lot fee-collection/management systems, gate access controls, and traffic monitoring systems. In addition, intelligent farming systems [2] are also under development in East-South Asia countries. Furthermore, smart ocean and ground shipment systems integrating satellite communications [3, 4] are under several discussions to provide seamless goods management.

Technologies to implement RFID systems have been categorized into low-frequency (LF), high-frequency (HF),

ultra-high-frequency (UHF), and microwave bands to fit the requirements in especially needed scenarios. The operational principles and functional mechanisms can be further classified into near- and far-field communications by using magnetic coupling [1] and electromagnetic (EM) wave induction [1, 5, 6] techniques to capture the required power, respectively. Due to the increasingly sophisticated application scenarios, integrating multiple heterogeneous RFID systems into a single system is necessary to simplify associated system architectures and make a compact size [2, 6]. In particular, a hybrid combination of near- and far-field RFID systems is essential to meet most RFID application needs, which require dual-band RFID antennas. For example, a novel smart button system has been introduced for fashion supply-chain tracking, which consists of near-field communication (NFC) and UHF RFID systems [2]. Note that the NFC tag is employed for customers to access the basic information of the product's historical records using their smartphone. In contrast, the UHF RFID tags can track products' identifications in shipping. To simplify the system complexity on the product sides, the tag antenna was designed to combine two bands by using an inductive spiral coil and a folded dipole for NFC and UHF RFID applications, respectively. Their received signals are processed by a dual-band tag chip [7]. Its performance has been validated to work well at 1.5 and 60 cm read ranges for NFC and UHF RFID applications, respectively. In addition, a unique tracking system for the supply chain of fresh vegetables was suggested by [8], where the dual bands of NFC and UHF RFID systems were used to record the store activity in the vegetable cultivation process and to perform the identification/traceability after harvest, respectively. Furthermore, [9] introduced the UHF HF RFID integrated tag for vehicle identification, where the RFID tag generally consists of an RFID tag chip, antenna, and encapsulation.

In the past, some researchers have introduced the dual-band RFID tag antenna. In [10], the dual-band tag antenna was designed to operate in 13.56 MHz and 868 MHz frequency bands with a credit card size on a polyimide substrate. The antenna structure consists of three parts in different layers. The top layer is a shorted-loop antenna. A center cutout and a narrow gap were created in the middle layer, while the bottom layer consists of a coil and substrate capacitor bridge gap. The tag antenna provides a quality factor of 54 at 13.56 MHz and a realized gain of -4.69 dBi at 868 MHz. In addition, a compact RFID tag antenna was also proposed on a single layer and operated at 13.56 MHz and 915 MHz [11]. The antenna structure employs a spiral coil for the HF band and a meander-line dipole for the UHF band, which is embedded inside the credit card-sized spiral coil. It has a good impedance match at 13.56 MHz and has a maximum realized gain of -5.36 dBi at 910 MHz [11].

On the other hand, the Hilbert curve [12] was proposed to design a dual-band RFID tag with a single radiator in a card type. The HF coil antenna was created using a series Hilbert curve, while the UHF antenna is a square loop structure. This antenna has a circular polarization with a realized gain of 1.75 dBi at 25 MHz, 2.65 dBi at 785 MHz, 2.82 dBi at 835 MHz, and 2.75 dBi at 925 MHz [12]. In addition, an integrated HF and UHF RFID tag antenna was introduced [13], which operates at 13.56 MHz and 920-925 MHz. The square spiral of the HF band is combined inside the CMA-based square loop for the UHF band. They can provide high magnetic field strength at 13.56 MHz and 0.31 dBic realized gain at 922.5 MHz. The maximum reading ranges are 4.9 cm and 8.7 m for HF and UHF bands, respectively. Other dual-band RFID tag antennas were also presented by other researchers [14–20]. Most dual-band RFID tags are in the credit card size of 53.98 mm in width and 85.6 mm in length, which is quite a large and complicated structure. Furthermore, the dual-band antenna finds applications in other exciting areas, as demonstrated in a real-time neural/EMG data acquisition system proposed in [21]. This system utilizes the dual-band antenna operating at 13.56 MHz (HF) and 915 MHz (UHF) frequencies for efficient power delivery in long-term implanted devices, where battery replacement is undesirable, and for high-speed backscatter communication.

Moreover, specific designs for dual-band RFID tag antennas are discussed in the literature. For instance, [22] presents the design of an ultrathin dual-band antenna on a metasurface for UHF RFID and WLAN applications. [23] focuses on a dual-band UHF RFID tag design to achieve a high read range. The utilization of an EBG structure in combination with the design of a dual-band RFID tag is explored in [24]. Additionally, [25] introduces a dual-band RFID tag design tailored explicitly for body temperature monitoring.

This research presents a dual-band RFID passive tag antenna design in a compact size to operate for identification, tracking, and traceability in a supply chain. The HF RFID is employed for customer checks by using their own smartphone and energy harvesting in the tag, and the UHF RFID is used for the shipping process management with the same RFID tag. The energy harvesting can be achieved at the HF band by the coupling magnetic field received by the HF antenna to the chip ST25DV04K at the output voltage pin. The antenna structure consists of a rectangular spiral coil for the HF band and a dipole with meander lines and patches for the UHF band. It is shorted at the end of the dipole for size reduction. Compared to the previous works, as shown later in Section 4, the proposed antenna has the advantages of a compact size of 26.92 mm in width and 67.84 mm in length (smaller than the credit card) and a low profile structure. It is easy to embed in any object within modern applications. In addition, the novelty of the proposed antenna is the appropriate interconnection of a rectangular spiral coil and a patch-meander-line dipole on a single-layer substrate with a shorted point to achieve the total size reduction with desirable antenna characteristics.

The rest of this paper is organized as follows. Section 2 discusses the antenna structure. Parametric studies and simulation results are shown in Section 3. Measurement results are provided in Section 4 for validation. Finally, conclusions are given in Section 5.

2. Antenna Structure

The proposed dual-band passive RFID tag antenna is implemented on a single-layer FR4 ($\varepsilon_r = 4.3$) dielectric substrate

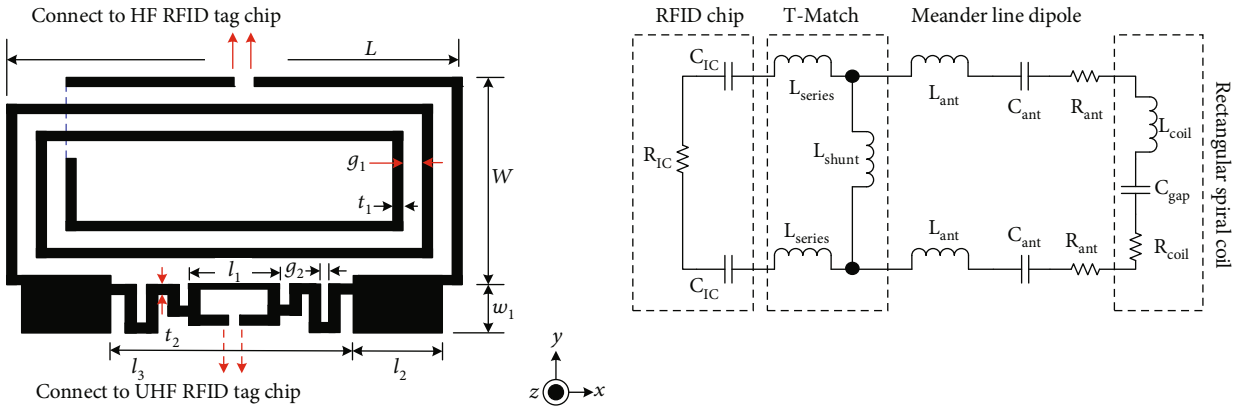

(a) Dual-band passive RFID tag antenna

(b) The equivalent circuit at the UHF band

Figure 1: The dual-band passive RFID tag antenna and equivalent circuit at the UHF band.

Table 1: Geometric parameters of dual-band passive RFID tag antenna.

Antenna parameter	Description	Size (mm)
W	The width of a spiral rectangular coil.	26.92
L	The length of a spiral rectangular coil.	67.84
g_1	The gap between the line of the rectangular spiral coil.	0.6
t_1	The thickness of the line of the rectangular spiral coil.	0.32
w_1	The width of the patch at the end of the meander-line dipole.	9
l_2	The length of the patch at the end of the meander-line dipole.	16
t_2	The thickness of the meander-line dipole.	1.5
g_2	The gap of the meander-line dipole.	0.5
l_1	The length of the loop on the meander-line dipole.	16
l_3	The length of the meander-line dipole.	33

for a low cost. The antenna structure consists of two essential parts to produce two resonant frequencies for HF and UHF RFID applications. In particular, the HF band resonance is produced by implementing a rectangular spiral coil of copper strips on the top section as shown in Figure 1(a). On the other hand, the UHF resonance is produced by a dipole architecture formed by a cascaded pair of patch and meander-line strips for size reduction. It is noted that, at the two patch terminations of the meander-line dipole, the HF spiral coils are connected, increasing the effective length of the spiral coil to produce a longer effective length for the spiral coils. Therefore, it reduces the resonant frequency to the lower HF band. This dual-band combination may make the antenna formation very compact. As a result, the resonance frequencies can achieve 13.56 and 922.5 MHz for the HF and UHF operations, respectively.

The proposed antenna incorporates two ports to accommodate the different RFID tag chips, enabling dual-band operations at widely separated frequencies. These tag chips, ST25DV04K [26] and SL3ICS1002 [27], are utilized for the HF and UHF bands at their respective ports. The design process becomes slightly more complex due to the combination of spiral coils and meander-line dipoles. Still, it significantly reduces the overall size of the antenna for improved compactness.

When considering impedance matching at the two excitations for the HF and UHF bands, it is crucial to consider the equivalent impedances of the spiral coils, meander-line dipoles, and the internal impedances of the tag chips. For instance, at the resonant frequencies, the HF tag chip has an internal capacitor of 28.5 pF [26], while the UHF tag chip exhibits an internal impedance of 22-j195 Ω [27]. These parameters play a crucial role in achieving proper impedance matching and efficient operation of the antenna across both frequency bands.

Additionally, Figure 1(b) illustrates the equivalent circuit of the dual-band passive RFID tag antenna. Based on the synthesis methodology described in [28], the antenna can be divided into three components to integrate the RFID chip: T-match network, meander-line dipole, and rectangular spiral coil. The RFID chip is represented by a series of resistors and capacitors (R_{IC} and C_{IC}). The T-match consists of inductors ($L_{series} = 7.5$ nH and $L_{shunt} = 18$ nH). The meander-line dipole comprises a series of RLC circuits ($L_{ant} = 20$ nH, $C_{ant} = 1$ nF, and $R_{ant} = 15\,\Omega$). Lastly, the rectangular spiral coil includes a series of inductor coils

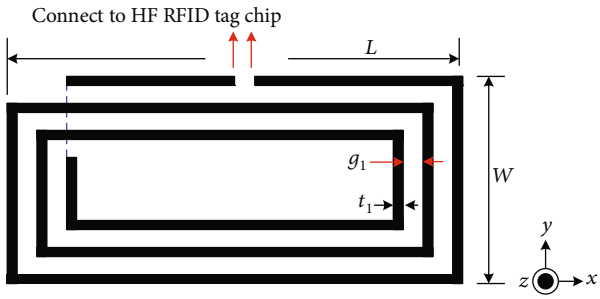

(a) Rectangular spiral coil

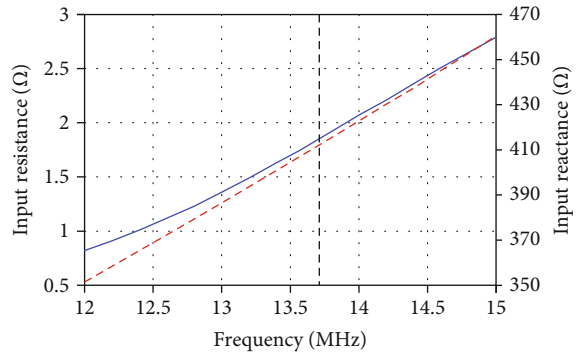

(b) Input resistance and reactance versus frequency

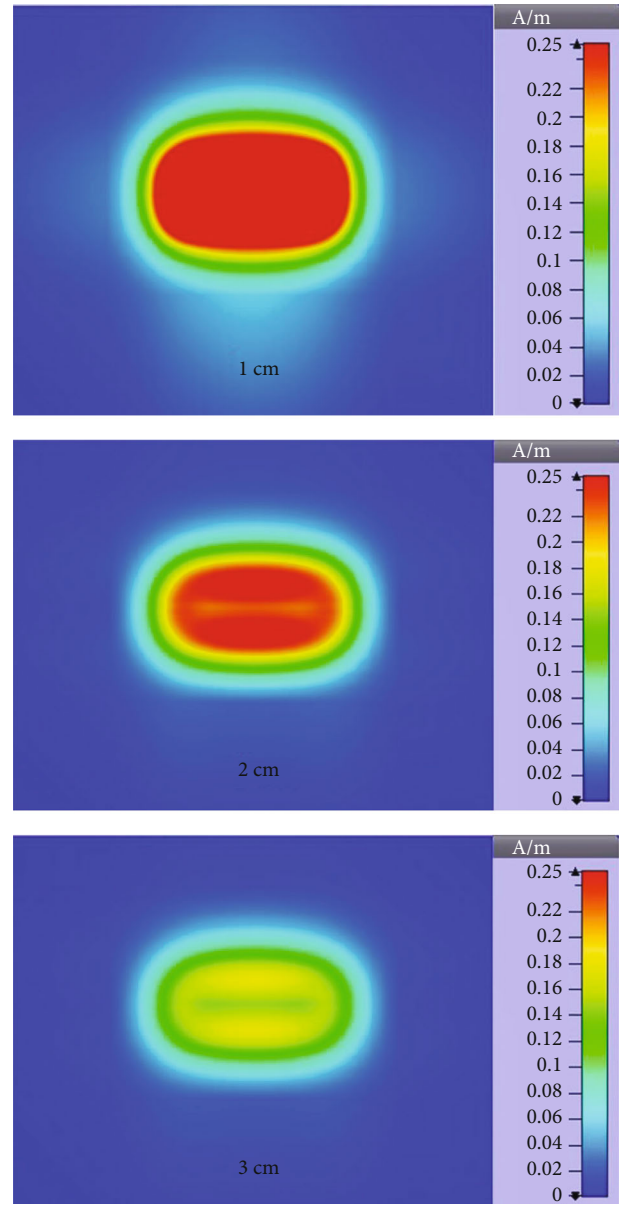

(d) Magnetic field intensity at 13.56 MHz

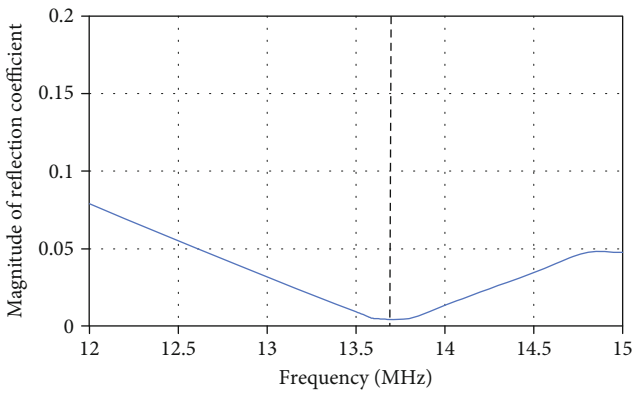

(c) Magnitude of reflection coefficient versus frequency

Figure 2: Simulation results of the rectangular spiral coil tag antenna for HF RFID applications.

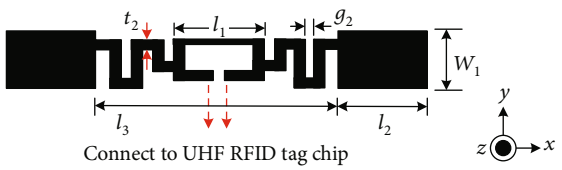

(a) Patch-meander-line dipole

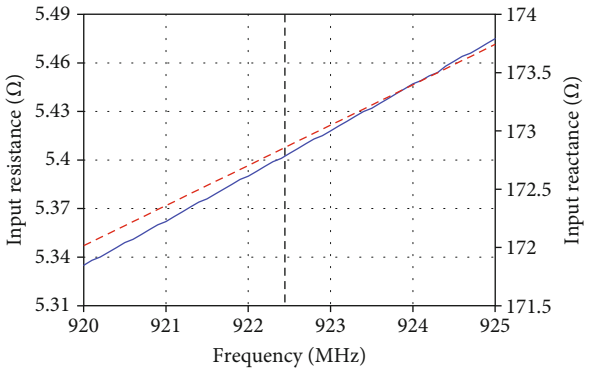

(b) Input resistance and reactance versus frequency

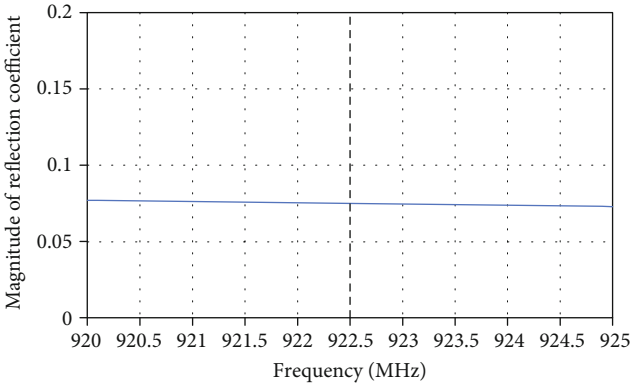

(c) Magnitude of reflection coefficient versus frequency

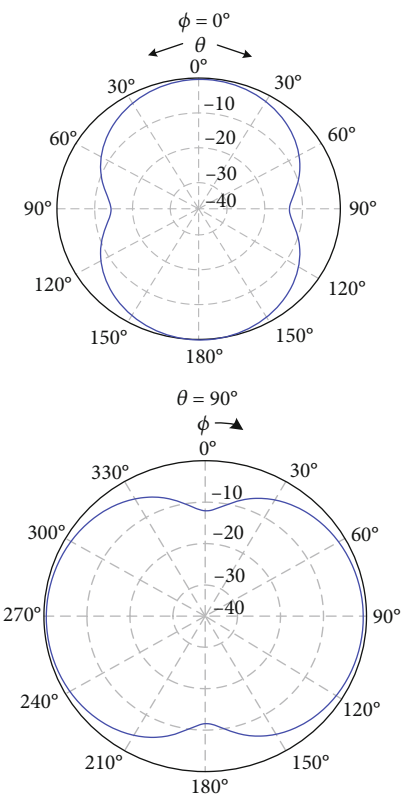

(d) Radiation patterns at 922.5 MHz

Figure 3: Simulated results of the patch-meander-line dipole for UHF RFID applications.

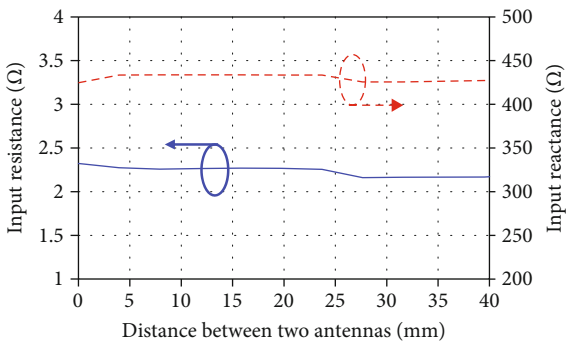

(a) Input resistance and reactance of the rectangular spiral coil versus the distance at 13.56 MHz

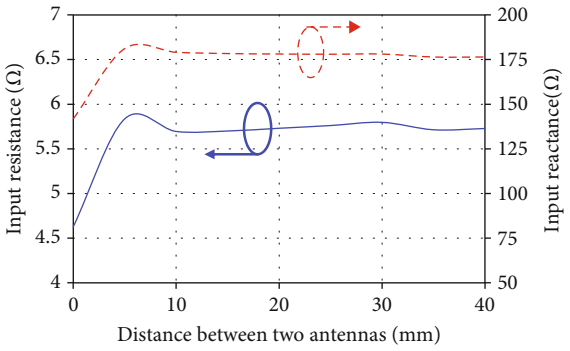

(b) Input resistance and reactance of the patch-meander-line dipole versus the distance at 922.5 MHz

Figure 4: Simulated input impedances versus the distance between the rectangular spiral coil and patch-meander-line dipole.

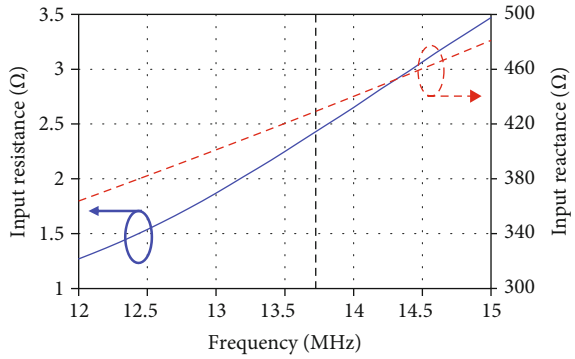

(a) Input resistance and reactance versus frequency at the HF band

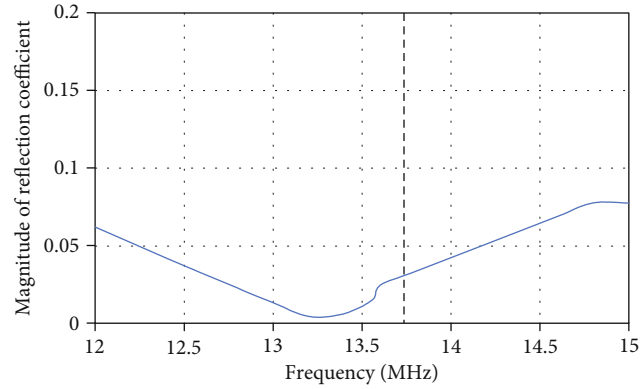

(b) Magnitude of reflection coefficient versus frequency

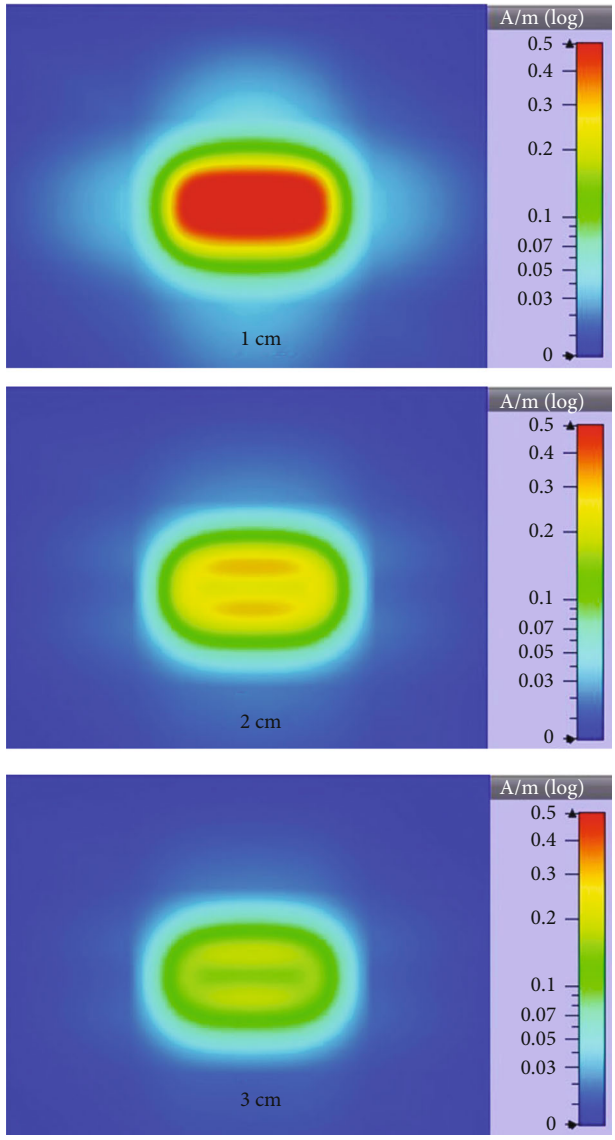

(c) Magnetic field intensity at 13.56 MHz

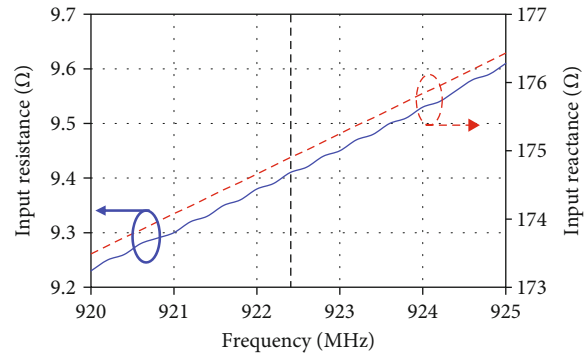

(d) Input resistance and reactance versus frequency at the UHF band

Figure 5: Continued.

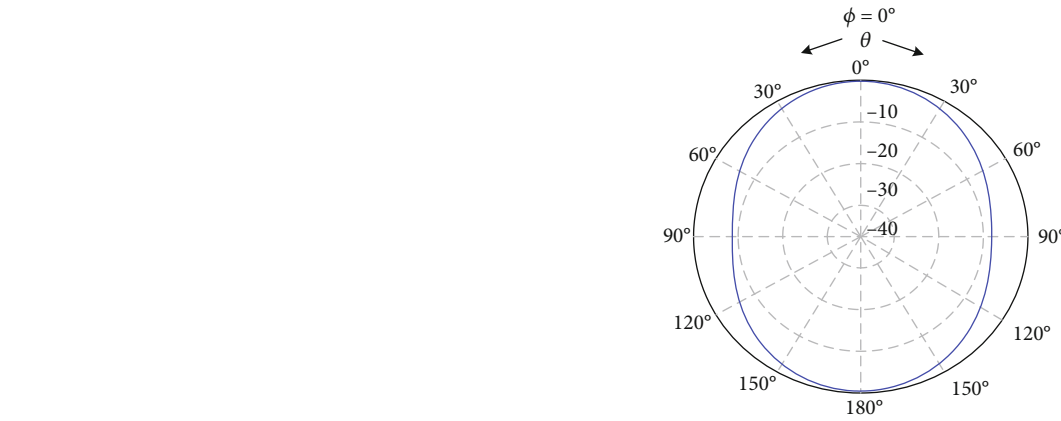

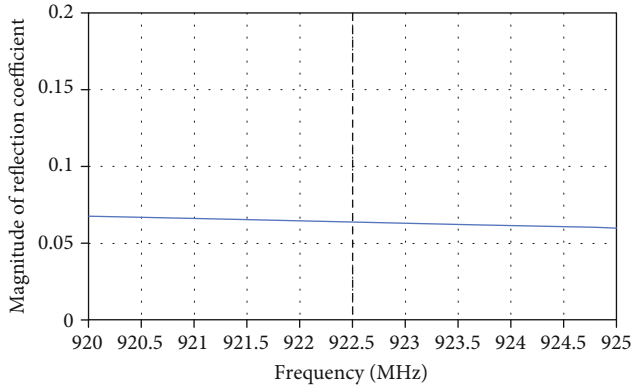

(e) Magnitude of reflection coefficient versus frequency

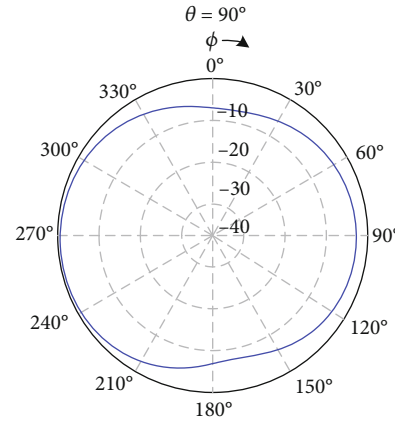

(f) Radiation patterns at 922.5 MHz

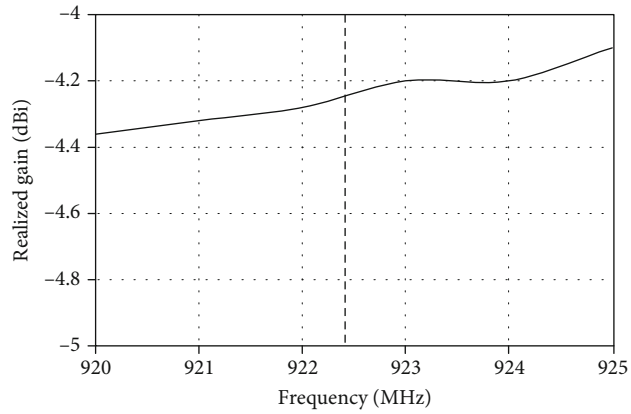

(g) Antenna realized gain at UHF band

Figure 5: Simulated results of the dual-band passive RFID tag antenna.

($L_{coil} = 25$ nH), capacitor coupling between coil gaps ($C_{gap} = 1$ nF), and resistor coils ($R_{coil} = 230\,\Omega$).

From an equivalent-circuit point of view, the combination of the spiral coil and patch-meander-line dipole on the same substrate produces field coupling between them and results in some effects on the self-impedance, which should be incorporated in the tag design consideration. Thus, in the design process, the shorted end of the UHF patch-meander-line dipole first implemented the impedance matching with the UHF chip, where the rule of conjugate matching was employed [29]. The position of this tag antenna is then placed outside the middle of the rectangular HF spiral coils to avoid magnetic field disturbance from the spiral coils in the near-field region. The later measurement validation demonstrated that the proposed antenna structure can provide a good reading range and energy harvesting. After numerous examinations by CST full-wave simulations [30], the geometric parameters' values of the antenna architecture were achieved as shown in Table 1 and used for prototype fabrication and measurement validation.

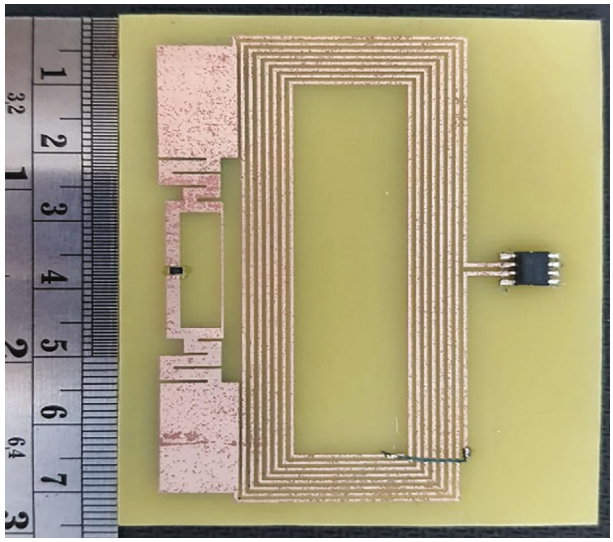

Figure 6: The prototype of the dual-band passive RFID tag antenna.

3. Numerical Simulations and Parametric Studies

The antenna structure was designed and implemented on an FR4 substrate with a dielectric constant of 4.3 and a substrate thickness of 1.6 mm. The copper to realize the antenna structure has a thickness of 0.001 mm. CST Microwave Studio [30] is employed to evaluate the proposed tag antenna. As shown in Figure 1, the tag antenna is formed by two parts to produce two resonances in the HF and UHF bands, including the rectangular spiral coil and the patch-meander-line dipole. They are on the top layer of the FR4 substrate and are arranged in the appropriate position. In the design process, the two HF and UHF structures were examined separately to exhibit their impedance and resonance behaviors for the two band resonances. The different effects are then combined to incorporate their impedances for an optimum design from a system point of view.

One first considers the HF rectangular spiral coils, as shown in Figure 2(a), where a straight strip replaces the UHF dipole part to form a complete rectangular spiral coil. Note that to create a full loop, the two end terminals in Figures 1 and 2(a) are shorted, as shown by the blue dashed line, such that the magnetic field can be well produced to extract the coupling current from the reader antenna's illumination. In the simulation, the antenna is modeled by copper strips in a rectangular shape. The internal capacitance of the RFID tag chip of ST25DV04K [26] is incorporated for impedance matching at 13.56 MHz for resonance. Since the internal capacitance is 28.5 pF, the tag antenna structure should produce an inductance of 4.83 μH to reach an inductive reactance of 411.83 Ω for the resonance at 13.56 MHz. After fine-tuning the geometric parameters in the CST simulations, the optimum width of the strip is 26 mm. Six rounds of the spiral loops were achieved to require a total length of 66 mm, which produces an inductance of 4.77 μH or inductive reactance of 406.67 Ω at 13.56 MHz with the strong magnetic field intensity as shown in Figures 2(b) and 2(d), respectively. For all relevant plots in this paper, the frequency markers (straight line) are also illustrated at the center frequencies of HF (13.56 MHz) and UHF (922.5 MHz) bands for clarity. It is seen that both the resistance and reactance vary linearly with the frequency. Higher values appear at higher frequencies, which are reasonable because, at a higher frequency, the aperture size also increases in wavelengths. In addition, the magnitude of the reflection coefficient (Γ) is shown in Figure 2(c), which is less than 0.1 with suitable impedance matching over the frequency of 12-15 MHz. In this case, the resistance is minimal, nearly 1-3 Ω to make the antenna structure inductive for good power coupling and less power loss. The reflection coefficient can be used as follows:

$$\Gamma = \frac{Z_{\text{antenna}} - Z^*_{\text{chip}}}{Z_{\text{chip}} + Z_{\text{antenna}}}, \tag{1}$$

where Z_{antenna} is the impedance of the tag antenna and Z_{chip} and Z^*_{chip} are the chip impedance and its complex conjugate. The effective coupling area and reasonable distance of antenna coupling can be seen from the magnetic field intensity distribution in Figure 2(d). The magnetic field intensity is normal to the antenna plane and decreases with the distance. It is seen that a short distance will provide a stronger magnetic field for coupling with a larger aperture area. In principle, putting the two tag and reader antennas as close as possible is desired. However, a close position causes rapid coupling variations. It makes impedance matching difficult because the sensitive variation at a very short distance requires accurate positioning of the two tag and reader antennas. As a result, a tradeoff should be considered in the design to provide good insensitivity in the allowable positioning range between the tag and reader antennas.

Next, the spiral coils were removed to retain only the patch-meander-line dipole for examination at the UHF band, where the resulting structure is shown in Figure 3(a). The tag antenna consists of a middle loop, a pair of meander lines, and two rectangular patches. In this case, the terminations of the dipole are the two rectangular patches. The meander line is in the middle between the patch and central loop to retain a low profile and compact size. The tag chip of SL3ICS1002 [27] is installed in the middle in a shunt connection to a strip line to form a loop for the operation at 920-925 MHz.

Based on the internal chip impedance of 22–j195 Ω, at the resonant frequency of 922.5 MHz, the appropriate antenna parameters are determined to provide a conjugate matching with the tag chip, where the antenna impedance is equal to $5.42 + j172.80\,\Omega$. The resulting tag antenna has the input impedance and radiates an omnidirectional with a realized gain of -5.38 dBi at 922.5 MHz as shown in Figures 3(b) and 3(d), respectively. Similar to the results in Figure 2(b), the input resistance and reactance of the antenna increase with frequencies. In this case, the input resistance is more significant than in Figure 2(b), while the input reactance is smaller. One should note that the

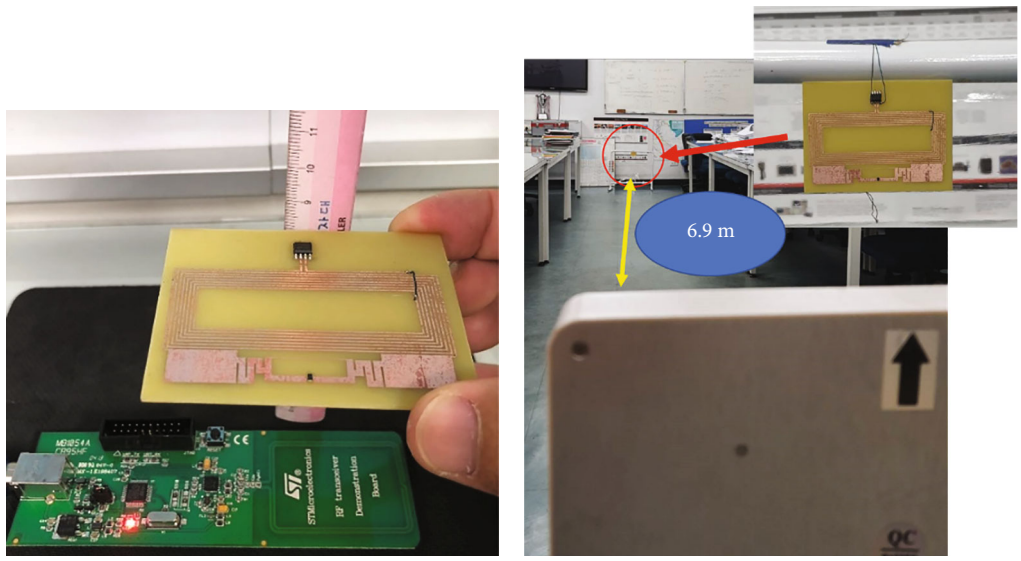

(a) HF band (b) UHF band

FIGURE 7: Measurement setups for RFID applications at the HF and UHF bands in (a) and (b), respectively. The measurements were performed at different separation distances between the reader and tag antennas.

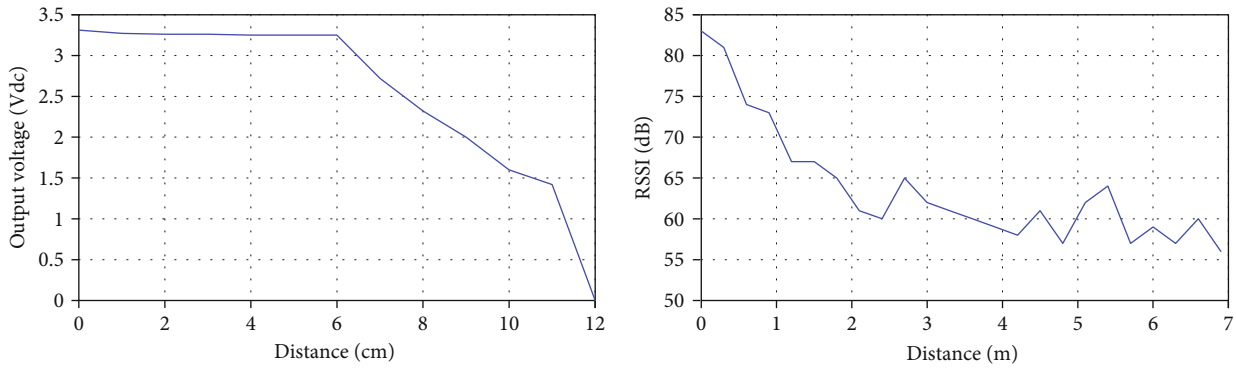

(a) HF band (b) UHF band

FIGURE 8: The measurements of the reading range for the dual-band passive RFID tag antenna.

considerable coupling mechanisms of the tag antenna at the HF and UHF bands are different. In addition, the magnitude of the reflection coefficient is shown in Figure 3(c), which is less than 0.1 with suitable impedance matching over the frequency range of 920-925 MHz.

A robust direct coupling at a short distance is required at the HF band to access the tag's data. On the other hand, in the UHF band, the reader antenna first radiates EM fields, which propagate to illuminate the tag antenna. In other words, in the HF band, the tag operates in the reactive near-field region such that the inductance is much more critical in extracting the signal power. In the UHF band, the tag antenna is in the propagation region, and the alignment of the antenna polarization is essential to acquire a good polarization loss factor [29]. The distance effects follow the fundamental nature of the power divergence along propagation. In such a case, the antenna realized gain is essential in focusing the radiation power along the tag direction. As shown in Figure 3(d), the radiation patterns of the tag antenna are bidirectional in the front and back sides, following the nature of a dipole antenna to focus the radiation on the cross-section plane.

Afterward, the two antenna structures are combined and put on the same substrate, which was introduced in [31] but is a separated antenna structure for HF and UHF bands. The combination arranges the patch-meander-line dipole outside the rectangular spiral coil. The patch ends of the dipole are shorted at the edge of the loop to form a complete dual-band antenna structure as shown in Figure 1 which is the interconnected structure. The individual impedance effects will alter the impedance match of each other at the two frequencies on the two chip ports. The target of the combination is to alleviate their impacts on each other's power transfer efficiencies, i.e., to reduce the mutual impedance from a circuit point of view. Impedance mismatches at these two frequencies should be compensated. Figures 4(a) and

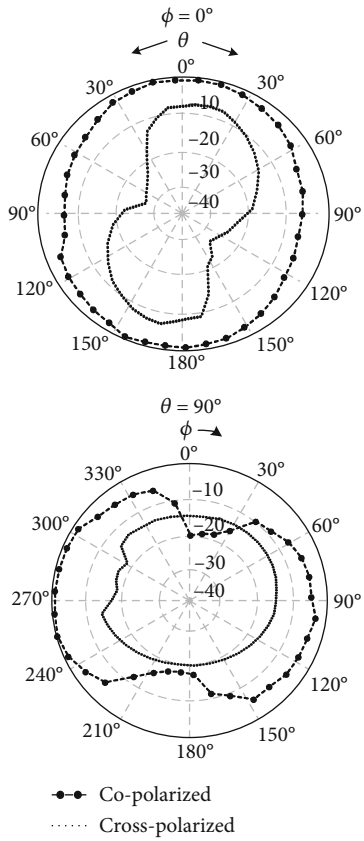

Figure 9: The measured radiation patterns for the dual-band passive RFID tag antenna at 922.5 MHz.

4(b) show the dual-band RFID tag antenna impedances at the two chip ports versus the distances at the two desired resonant frequencies for the rectangular spiral coil and patch-meander-line dipole, respectively. Compared to Figure 2(b), the input resistance in Figure 4(a) increases to more than 2 Ω, which might increase power loss and cause an impedance mismatch and lower the power transfer efficiency. Similar impedance-matching problems appear in the UHF band as well. It is seen from Figure 4(b) that the input resistance and the input reactance slightly swing. However, the deviation ratios at most distances are less than in the HF band because the radiation mechanism for power transfer is less sensitive. A proper distance is essential, where 1 mm is selected for the combination of these two antenna sections, and the patch ends of the dipole are shorted at the edge of the loop.

The input impedances of the combined tag antenna can be controlled by optimizing the number of coils for the HF band and the patch/meander-line for the UHF band. Simulation results indicate that the dual-band tag antenna exhibits an inductance of 4.96 μH or an inductive reactance of 422.79 Ω at 13.56 MHz, as shown in Figures 5(a) and 5(b). At 922.5 MHz, the antenna demonstrates an impedance of $9.41 + j174.96\,\Omega$, as shown in Figures 5(d) and 5(e). Note that Figures 5(b) and 5(e) show the magnitude of the reflection coefficient for the dual-band tag antenna in HF (12-15 MHz) and UHF (920-925 MHz) bands. There is a good match between the antenna, and both tag chips can be achieved. Moreover, the power transmission coefficient (PTC: τ) is computed using the associated formula given in [32].

$$\tau = 1 - |\Gamma|^2, \tag{2}$$

where it is found that the PTC is approximately 1 due to the low magnitude of the reflection coefficient over the operating frequency of 12-15 MHz and 920-925 MHz. Through proper parametric optimization, Figures 5(c) and 5(f) illustrate the dual-band RFID tag antenna's magnetic field intensity and radiation patterns at 13.56 MHz and 922.5 MHz, respectively. It can be observed that the tag antenna radiates a magnetic field in the normal direction of the loop, reaching a maximum intensity of 0.5 A/m at 13.56 MHz (at a distance of 1 cm). At 922.5 MHz, the antenna generates omnidirectional far-field radiation patterns with a realized gain of -4.26 dBi. Notably, the realized gain at 922.5 MHz is improved by more than 1 dB or over 20%. Figure 5(g) shows the antenna realized gain versus the frequency in the UHF band, which is from -4.4 to -4.1 dBi. Conversely, at 13.56 MHz, the power distribution is concentrated in the reactive near-field region.

The simulation results show that the dual-band passive RFID tag antenna provides the maximum magnetic field intensity equal to 0.5 A/m normal to the antenna. It can be conjugately matched with the chip with an inductance of 4.96 μH. In the UHF band, the proposed antenna provides a realized gain of -4.26 dBi at 922.5 MHz with an omnidirectional radiation pattern. Note that the antenna has suitable impedance matching with the chips at these two frequency bands.

To estimate the RFID tag performance in the application, the read range is considered especially in the UHF band. The Friis transmission equation is employed as shown in [33]

$$P_r^{\text{tag}}(\text{dB}) = P_t^{\text{reader}}(\text{dB}) + G^{\text{reader}}(\text{dB}) + G^{\text{tag}}(\text{dB}) - 20\log_{10}\left(\frac{4\pi R}{\lambda}\right), \tag{3}$$

where P_t^{reader} is the transmitted power of the reader (30 dBm), P_r^{tag} is the activation power of the tag chip tag (-15 dBm), G^{reader} and G^{tag} are the gain of reader and tag antennas (6 dBi and -4.26 dBi), respectively, λ is the wavelength at the operating frequency (922.5 MHz), and R is the read range. It is found that the theoretical read range is approximately 5.61 m, which is close to the measured result of 6.9 m. In addition, the theoretical read range at the HF band can be found by varying the distance and using the simulated magnetic field intensity, which is found that the magnetic field intensity is decayed to 0.15 A/m (the activation field strength of the chip) at 8 cm, which is close to the measured result of 11 cm.

Table 2: Comparison of the proposed dual-band RFID tag antenna with previous works.

Reference	Size (mm^2)	Antenna structure	Freq. band (MHz)	Pol.	Realized gain (dBi)
Mayer and Scholtz [10]	85.6 × 53.98 (credit card size)	Coil and shorted loop in multilayer	13.56/868	Linear	-4.69 @ 868
Ma et al. [11]	85.6 × 53.98 (credit card size)	Spiral coil and meander-line dipole combination on a single layer	13.56/915	Linear	-5.36 @ 915
Kenari et al. [12]	85.6 × 53.98 (credit card size)	Series Hilbert curve and square loop in a single layer	25/785/ 835/925	Circular	0.75 @ 25, 2.65 @ 785, 2.82 @ 835 2.75 @ 925
Sakonkanapong and Phongcharoenpanich [13]	95 × 95	Square spiral and CMA-based square loop combination in a single layer	13.56/922.5	Circular	1.67 @ 922.5
Farahani et al. [14]	30 × 50	Square spiral and meander line in a single layer	13.56/860	Linear	-1 @ 860
Phatarachaisakul et al. [15]	54 × 84	Square spiral and meander-line dipole in a single layer	13.56/922.5	Linear	0.62 @ 922.5
Nishioka et al. [16]	85.6 × 53.98 (credit card size)	Coil and monopole combination in a single layer	13.56/953	Linear	1 @ 953
Proposed antenna	67.84 × 26.92	Coil and patch-meander-line dipole in a single layer with a shorted point	13.56/922.5	Linear	-4.26 @ 922.5

4. Measured Results

The prototype of the tag antenna is fabricated for measurement validation, where the HF and UHF RFID chips are both implemented on the tag antenna, as shown in Figure 6. The two chips are SL3ICS1002 [27] for the UHF RFID (XSON3 package) and ST25DV04K [26] for the HF RFID (SO8N package). The prototyped tag antenna is measured for the input impedances without the RFID chips using a coaxial balun for both HF and UHF frequencies. It is found that its input impedances are equal to $15.49 + j307.23\,\Omega$ at 13.56 MHz with the PTC τ of 0.98 and $4.62 + j108.34\,\Omega$ at 922.5 MHz with τ of 0.91. Note that the simulated τ at 13.56 and 922.5 MHz are both equal to 0.99, which agree quite well with the measured τ. In addition, the tag antenna is evaluated by measuring the maximum read ranges with the RFID readers at 13.56 MHz and 922.5 MHz. Note that the energy harvesting can be achieved by using the power transfer from the magnetic field received by the HF antenna to the chip ST25DV04K at the output voltage pin. The measurement setups are shown in Figures 7(a) and 7(b) for the HF and UHF bands, respectively, where the measurements were performed at various distances. One can measure the output voltage at the HF band versus the separation distance between the reader and tag antennas. On the other hand, a long meter-scale distance is considered the separation distance above, where the reading data of received-signal-strength-indicator (RSSI) signal strengths were measured from an RFID system.

In the experiment, the UHF band employed the R2000 RFID reader, while the HF band used the STMicroelectronics RFID reader. The measured data from both readers are presented in Figure 8. During the measurement process, the dual-band passive RFID tag antenna was gradually moved away from the RFID reader in a line-of-sight manner. The RFID reader displayed the read tag status and RSSI (UHF) or the output voltage pin of energy harvesting (HF) for each distance. Note that the output voltage is achieved by the magnetic field coupling at the HF antenna to the chip ST25DV04K, where this magnetic field is converted to the voltage for the chip activation and energy harvesting.

Figure 8(a) illustrates that in the HF band, when the distance is less than 6 cm, the output voltages are relatively high, approximately 3.3 Vdc, and remain relatively consistent. Beyond this distance, the output voltage gradually decreases and reaches nearly zero at 12 cm, indicating a maximum read range of 11 cm in the HF band. On the other hand, in the UHF band, the measured RSSI decreases with increasing distance due to the natural power divergence along the propagation of the electromagnetic wave from the reader. Some oscillations are observed, which can be attributed to environmental scattering interferences. It should be noted that even at distances longer than 6.9 m, the RSSI remains above 56 dB. The polarization of the reader and tag antennas was manually aligned to ensure good polarization matching. In addition, the measured radiation patterns at 922.5 MHz are shown in Figure 9, exhibiting an omnidirectional radiation pattern with the realized gain of -3 dBi, which is close to the simulated one of -4.26 dBi with low cross-polarization. Note that they are in good agreement with the simulated results in Figure 5(f).

Finally, the performances of the proposed dual-band passive RFID tag antenna are compared to the past works reported in the literature, as shown in Table 2. It is seen that the proposed tag antenna has the smallest physical size among the comparison works. The two frequencies of RFID that we prefer to use in the design are HF (13.56 MHz) and UHF (860-960 MHz) due to many applications in those bands. Most of the tag antenna structures employ the spiral coil for operation at 13.56 MHz, which can be effective in coupling the magnetic field, and the square loop, dipole, and monopole with meander line are employed for operation at 860-960 MHz, where they are the compact size and omnidirectional radiation pattern. Most applications need

the physical structure as in a card type, and they are designed within the size of a credit card. From the results, the tag antenna has a low antenna realized gain and can be linear and circular polarization. The proposed antenna has the advantages of a dual-band RFID tag with a compact size of 26.92 mm in width and 67.84 mm in length, smaller than the credit card and low profile structure. It is easy to embed in any object within modern applications. In addition, the proposed antenna appropriately combines a rectangular spiral coil and patch-meander-line dipole on a single-layer substrate with a shorted point.

5. Conclusions

The dual-band RFID tag antenna combines a rectangular spiral coil and patch-meander-line dipole antennas with an interconnected structure. Through simulations, it has been determined that the antenna can operate effectively in both HF (13.56 MHz) and UHF (920-925 MHz) RFID systems. The proposed tag antenna ensures conjugate impedance matching with the two RFID tag chips, exhibiting an inductance of 4.96 μH or inductive reactance of 422.79 Ω at 13.56 MHz, as well as an impedance of 9.41 + j174.96 Ω at 922.5 MHz.

The dual-band RFID tag antenna's magnetic field intensity and radiation patterns were studied at 13.56 MHz and 922.5 MHz. The results demonstrate that the tag antenna emits a magnetic field in the normal direction of the loop, with a maximum intensity of 0.5 A/m at 13.56 MHz (at a distance of 1 cm). At 922.5 MHz, the antenna exhibits omnidirectional far-field radiation patterns, achieving a realized gain of -4.26 dBi. In addition, a prototype of the tag antenna was fabricated and tested with two RFID readers. The measurements revealed maximum read ranges of 11 cm for the HF band, accompanied by 1.48 volts of energy harvesting for the HF band, and 6.9 m for the UHF band.

Data Availability

Data sharing is not applicable to this article as no datasets were generated or analyzed during the current study.

Conflicts of Interest

The authors declare that they have no conflicts of interest.

Acknowledgments

This research was funded by the King Mongkut's University of Technology North Bangkok (contract no. KMUTNB-65-KNOW-12) and the National Science and Technology Council, Taiwan.

References

[1] R. Want, "An introduction to RFID technology," *IEEE Pervasive Computing*, vol. 5, no. 1, pp. 25–33, 2006.

[2] P. Mezzanotte, V. Palazzi, F. Alimenti, and L. Roselli, "Innovative RFID sensors for Internet of Things applications," *IEEE Journal of Microwaves*, vol. 1, no. 1, pp. 55–65, 2021.

[3] G. Benelli, A. Pozzebon, G. Raguseo, D. Bertoni, and G. Sarti, "An RFID based system for the underwater tracking of pebbles on artificial coarse beaches," in *2009 Third International Conference on Sensor Technologies and Applications*, pp. 294–299, Athens, Greece, 2009.

[4] M. Katayama, H. Nakada, H. Hayashi, and M. Shimizu, "Survey of RFID and its application to international ocean/air container tracking," *IEICE Transactions on Communications*, vol. 95, no. 3, pp. 773–793, 2012.

[5] A. A. Brahim, K. Nisar, Y. K. Hzou, and I. Welch, "Review and analyzing RFID technology tags and applications," in *2019 IEEE 13th International Conference on Application of Information and Communication Technologies (AICT)*, Baku, Azerbaijan, 2020.

[6] A. Haibi, K. Oufaska, K. El Yassini, M. Boulmalf, and M. Bouya, "Systematic mapping study on RFID technology," *IEEE Access*, vol. 10, pp. 6363–6380, 2022.

[7] E. M. Microelectronic, "Dual frequency NFC type 2 & EPC GEN2 V2 transponder IC," https://vyvoj.hw.cz/files/4423_datasheet.pdf.

[8] L. Mainetti, F. Mele, L. Patrono, F. Simone, M. L. Stefanizzi, and R. Vergallo, "An RFID-based tracing and tracking system for the fresh vegetables supply chain," *International Journal of Antennas and Propagation*, vol. 2013, Article ID 531364, 15 pages, 2013.

[9] A. Toccafondi, C. D. Giovampaola, F. Mariottini, and A. Cucini, "UHF-HF RFID integrated tag for moving vehicle identification," in *2009 IEEE Antennas and Propagation Society International Symposium*, North Charleston, SC, USA, 2009.

[10] L. W. Mayer and A. L. Scholtz, "A dual-band HF/UHF antenna for RFID tags," in *2008 IEEE 68th Vehicular Technology Conference*, Calgary, AB, Canada, 2008.

[11] Z. L. Ma, L. J. Jiang, J. Xi, and T. T. Ye, "A single-layer compact HF-UHF dual-band RFID tag antenna," *IEEE Antennas and Wireless Propagation Letters*, vol. 11, pp. 1257–1260, 2012.

[12] M. A. Kenari, M. N. Moghadasi, R. A. Sadeghzadeh, B. S. Virdee, and E. Limiti, "Dual-band RFID tag antenna based on the Hilbert-curve fractal for HF and UHF applications," *IET Circuits, Devices & Systems*, vol. 10, no. 2, pp. 140–146, 2016.

[13] A. Sakonkanapong and C. Phongcharoenpanich, "Near-field HF-RFID and CMA-based circularly polarized far-field UHF-RFID integrated tag antenna," *International Journal of Antennas and Propagation*, vol. 2020, Article ID 6427157, 15 pages, 2020.

[14] H. S. Farahani, B. Rezaee, M. Gadringer et al., "A miniaturized HF/UHF dual-band RFID tag antenna," in *2021 IEEE International Symposium on Antennas and Propagation and USNC-URSI Radio Science Meeting (APS/URSI)*, pp. 383-384, Singapore, 2022.

[15] T. Phatarachaisakul, T. Pumpoung, P. Wongsiritorn, R. Pansonboon, and C. Phongcharoenpanich, "Printed antenna for HF- and UHF-RFID tag," in *2014 International Symposium on Antennas and Propagation Conference Proceedings*, pp. 513-514, Kaohsiung, Taiwan, 2015.

[16] Y. Nishioka, K. Hitomi, H. Okegawa et al., "Design and evaluation of HF/UHF dual-band RFID tag utilizing HF-coil as UHF antenna conductor," in *2014 IEEE-APS topical conference on antennas and propagation in wireless communications (APWC)*, pp. 225–228, Palm Beach, Aruba, 2014.

[17] J. Xi and C.-L. Mak, "A compact dual band RFID metal tag with orthogonal polarizations at ETSI and FCC bands," in *2017 IEEE International Conference on RFID Technology & Application (RFID-TA)*, pp. 130–133, Warsaw, Poland, 2017.

[18] F. Amato and S. Hemour, "The harmonic tunneling tag: a dual-band approach to backscattering communications," in *2019 IEEE International Conference on RFID Technology and Applications (RFID-TA)*, pp. 244–247, Pisa, Italy, 2019.

[19] J. Liu, "Dual-band RFID tag antenna using coplanar inverted-F/L structure," in *2010 IEEE International Conference on RFID-Technology and Applications*, pp. 96–99, Guangzhou, China, 2010.

[20] W. Pachler, J. Grosinger, W. Bösch, G. Holweg, and C. Steffan, "A miniaturized dual band RFID tag," in *2014 IEEE RFID technology and applications conference (RFID-TA)*, pp. 228–232, Tampere, Finland, 2014.

[21] E. Kampianakis, A. Sharma, J. Arenas, and M. S. Reynolds, "A dual-band wireless power transfer and backscatter communication approach for real-time neural/EMG data acquisition," *IEEE Journal Of Radio Frequency Identification*, vol. 1, no. 1, pp. 100–107, 2017.

[22] S. Sarkar and B. Gupta, "Ultrathin dual-band metasurface for UHF-RFID and WLAN applications," in *2021 IEEE International Conference on RFID Technology and Applications (RFID-TA)*, pp. 101–104, Delhi, India, 2021.

[23] A. Bansal, S. Sharma, and R. Khanna, "RFID tag design with high read range performance for dual band applications in UHF range," in *2022 IEEE 12th International Conference on RFID Technology and Applications (RFID-TA)*, pp. 82–85, Cagliari, Italy, 2022.

[24] T. Phatarachaisakul, T. Pumpoung, and C. Phongcharoenpanich, "Dual-band RFID tag antenna with EBG for glass objects," in *2015 IEEE 4th Asia-Pacific conference on antennas and propagation (APCAP)*, pp. 199-200, Bali, Indonesia, 2016.

[25] B. Liu, Y. Li, B. Huang, J. Li, and H. Liu, "A compact HF-UHF dual-band wearable RFID tag for body temperature monitoring," in *2022 IEEE MTT-S International Microwave Workshop Series on Advanced Materials and Processes for RF and THz Applications (IMWS-AMP)*, Guangzhou, China, 2013.

[26] Dynamic NFC/RFID tag IC, *ST25DV04K, DS10925- Rev 9*, 2021, http://www.st.com/.

[27] UCODE, G2XM, and G2XL, *SL3ICS1002/1202, rev. 3.8*, NXP Semicoenductors, 2013.

[28] G. Zamora, S. Zuffanelli, F. Paredes, F. Martin, and J. Bonache, "Design and synthesis methodology for UHF-RFID tags based on the T-match network," *IEEE Transactions on Microwave Theory and Techniques*, vol. 61, no. 12, pp. 4090–4098, 2013.

[29] C. A. Balanis, *Antenna Theory: Analysis and Design*, John Wiley & Sons, 3rd edition, 2016.

[30] D. Systèmes, "CST studio suite 2012, Dassault Systèmes," 2012, https://www.3ds.com/products-services/simulia/products/cst-studio-suite/solvers/.

[31] T. Mhunkaew, S. Kawdungta, and D. Torrungrueng, "Dual-band UHF and HF-RFID tag antenna for tracking and energy harvesting applications," in *2023 International electrical engineering congress (iEECON)*, pp. 72–75, Krabi, Thailand, 2023.

[32] Y. Shafiq, J. S. Gibson, H. Kim, C. P. Ambulo, T. H. Ware, and S. V. Georgakopoulos, "A reusable battery-free RFID temperature sensor," *in IEEE Transactions on Antennas and Propagation*, vol. 67, no. 10, pp. 6612–6626, 2019.

[33] H. Peter, Z. Hu, and Y. Wang, "Operating range evaluation of RFID systems," in *Advanced Radio Frequency Identification Design and Applications*, InTech, 2011.